Upconversion in Er^{3+}:ZrO_2 Nanocrystals

Amitava Patra, Christopher S. Friend, Rakesh Kapoor, and Paras N. Prasad*

Institute for Lasers, Photonics and Biophotonics, University at Buffalo, The State University of New York, Buffalo, New York 14260

Received: September 19, 2001

Erbium-doped ZrO_2 nanoparticles are prepared by a sol−emulsion−gel technique. The effects of the Er^{3+} concentration and different codopants (Yb^{3+} and Y^{3+}) in the ZrO_2 matrix on the upconverted emission are reported. Green and red upconversion emission at 550 and 670 nm were observed from these oxide nanocrystals with 980 nm excitation. The overall intensity decreases with an increasing concentration of erbium in zirconia. The presence of codopants (Y^{3+} and Yb^{3+}) also increases the overall intensity of the upconverted emission. The emission spectra and the pump intensity dependence of the luminescence intensities are used to understand the excitation mechanism. These results confirm that upconverted emission in these materials is due to a two-photon excited-state absorption (ESA)/energy transfer upconversion (ETU) process.

1. Introduction

Rare-earth ions, especially erbium, have played an important role in the development of optical communication technology during the past few decades. Recently, erbium-doped luminescent materials have received considerable attention for frequency upconversion of infrared radiation into the visible region.[1−8] A variety of potential applications to lasers, displays, and two-photon fluorescence imaging[1−8] are possible with the suitable selection of a host matrix and the rare-earth dopant ion concentration. The local environment, the dopant concentration, and the distribution of active ions in a host material affect the upconversion efficiency. It is well established that in the luminescence of rare-earth ions the highest phonon frequencies of the host lattice are responsible for nonradiative relaxations.[9] In accordance with the energy law, the presence of a large gap between emitting and terminal levels reduces the probability of nonradiative decay. A lower host phonon energy has a greater number of phonons connecting the emitting level with the next lower level. The more phonons needed to gap the energy will decrease the nonradiative relaxation probability and increase the quantum yield of luminescence. To overcome the phonon decay problem it is necessary to choose a lattice that has a much lower phonon energy. The zirconia matrix seems to be an ideal medium for preparation of highly luminescent materials because it is chemically and photochemically stable, has a high refractive index and a low phonon energy.[10] The stretching frequency of the zirconia matrix is about 470 cm^{-1}, which is much lower than for Al_2O_3 (870 cm^{-1}) or SiO_2 (1100 cm^{-1}) but higher than for Y_2O_3 (300−380 cm^{-1}). Nanoparticles, on the other hand, have recently been recognized to hold tremendous potential in the area of photonic applications. The special interest in nanoparticles of these materials relates to enhanced intensity of emission detected for smaller size particles.[11] Combining the promising optical properties of rare-earth ions and nanoparticles, the study of frequency upconversion processes of erbium in zirconia nanoparticles is important.

Various chemical methods have been developed to control the size and distribution of nanoparticles during synthesis. Due to the high surface area and the surface energy, the nanoparticles undergo aggregation into larger particles. In conventional methods, uncontrolled nucleation and subsequent growth of the precipitated particles in a bulk aqueous medium finally generates larger particles with a wide size distribution. To overcome these problems, many recent studies have used emulsions to control the size and morphology of the nanoparticles.[12−15] Generally the reverse micelles formed in water-in-oil (w/o) type emulsions act as the micro- or nano-reactors in which reactions are carried out.[12,13] It is known that a minimum critical micelle concentration (cmc) is needed for the surfactant molecules to self-aggregate, giving rise to "reverse micelles" in organic solvents. Here, we use a sol−emulsion−gel process to prepare zirconia nanoparticles doped with Er. The principle of the process involves the dispersion of a sol containing the desired constituents under agitation into a water-immiscible organic liquid for low dielectric constant. To stabilize the dispersed sol droplets, addition of an amphiphilic surface-active agent is necessary. Gelation of the sol droplets with a suitable gelling agent produces gel particles.

In the present work, we have prepared Er^{3+}:ZrO_2 nanoparticles by using a sol−emulsion−gel technique and the effect of concentration of erbium ions and codopants on upconversion emission has been studied.

2. Experimental Procedure

The sol−emulsion−gel method was used for the preparation of Er^{3+}-doped ZrO_2 nanoparticles. Zirconia propoxide (Fluka) and erbium acetate were used as the starting materials. First, 3 mL of glacial acetic acid was slowly added to 10 mL of zirconia propoxide and stirred for 30 min. Then 20 mL of *n*-propanol was added to the solution, which was further stirred for 15 min at room temperature. A volume of 4 mL of 50% aqueous acetic acid was slowly added to the above solution under stirring which resulted in a clear transparent solution. Then, a stoichiometric amount of erbium acetate was added to this solution. The emulsified sol droplets were obtained through water-in-oil (w/o) type emulsions with cyclohexane and sorbitan monooleate (Span 80, fluka) as the organic liquid (oil phase) and nonionic surfactant, respectively. The support solvent containing 5 vol

* Author to whom correspondence should be addressed.

10.1021/jp013576z CCC: $22.00
Published on Web 02/02/2002

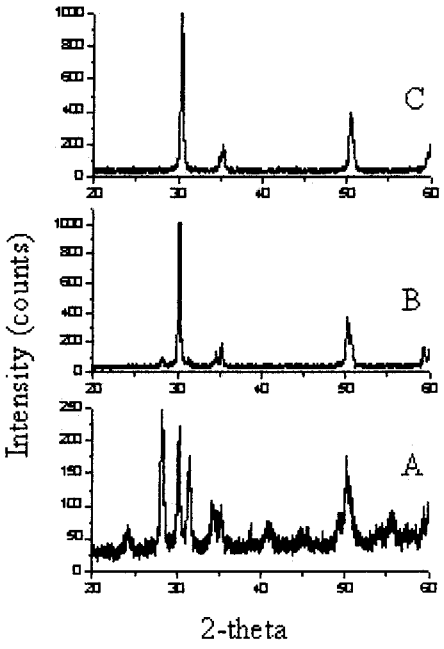

Figure 1. Powder X-ray diffraction patterns of ZrO_2 nanoparticles obtained after heating at 1000 °C. A (0.25 Er^{3+}), B (0.25 Er^{3+} + 0.25 Yb^{3+}), C (1.0 Er^{3+} + 1.5 Y^{3+}).

% of span 80 in cyclohexane was used for emulsification, i.e., for the preparation of a water-in-oil (w/o) type emulsion in the present study. The volume ratio of the sol and cyclohexane was 1:4. A measured amount of erbium-doped zirconia sol was then dispersed in the solvent under stirring condition. The sol droplets formed in the process were then gelled by the controlled addition of a base. The gel particles were separated by centrifugation followed by washing with acetone and methanol. The product was dried at 60 °C in air for 12 h. The dried materials were ground and calcined at 1000 °C for 1 h.

Transmission electron microscopy (TEM) was employed to determine the morphology and the particle size of the resulting powders; the crystalline phases of calcined powders were identified by X-ray diffraction (XRD). X-ray powder diffraction patterns of the different samples at 1000 °C were recorded. The crystallite sizes of the nanoparticles were calculated following the Scherrer's equation:

$$D = K\lambda/\beta \cos \Theta \qquad (1)$$

where $K = 0.9$, D represents crystallite size (A), λ represents the wavelength of Cu kα radiation, and β represents the corrected half width of the diffraction peak. We pressed the particles to form a smooth, opaque flat disk for optical study. The samples were irradiated with a diode laser tuned to 975 nm. A CCD-coupled spectrometer recorded the fluorescence spectra. The absolute fluorescence intensity was measured with a Minolta LS-110 Luminance meter.

3. Results and Discussion

3.1. Structural Investigations. The powder X-ray diffraction patterns in Figure 1 indicate the crystallization of zirconia nanoparticles of different compositions at 1000 °C. The powder XRD patterns show the presence of both monoclinic and tetragonal phases for low dopant concentration and cubic at higher dopant concentration. The crystallite size (27−50 nm) varies with the composition. Figure 2 shows the TEM picture of the ZrO_2 nanoparticles. A small deviation in the estimated particle sizes by TEM and X-ray diffraction may result since

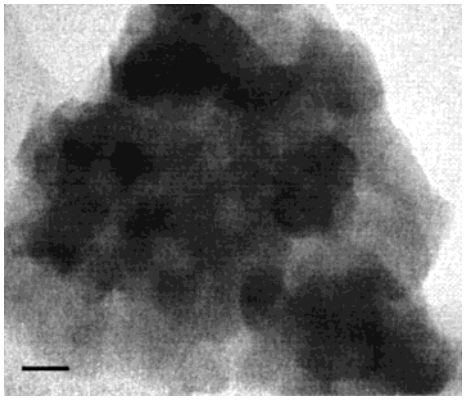

Figure 2. Transmission electron micrographs of ZrO_2 nanoparticles obtained after heating at 1000 °C (bar is 20 nm).

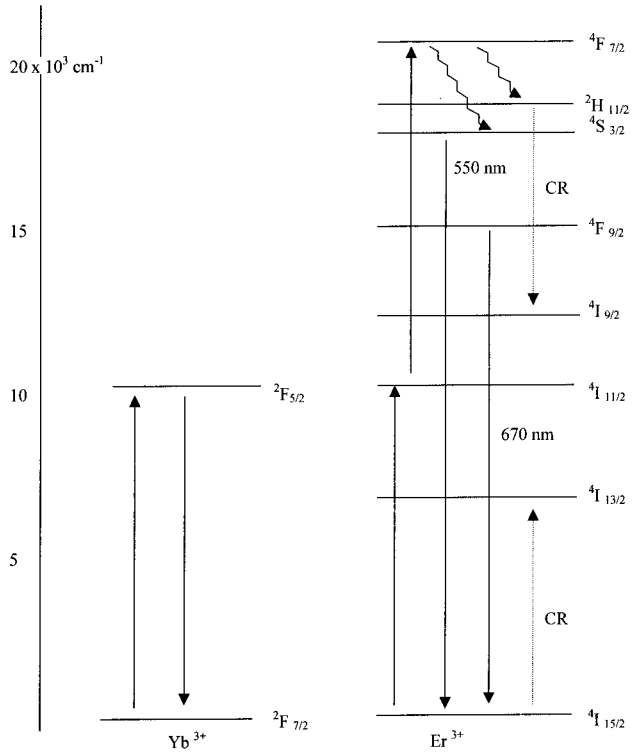

Figure 3. The energy level diagram for Yb^{3+} and Er^{3+} ions under infrared excitation.

XRD refers to coherent domains and the TEM images may be polydomain in nature.

3.2. Upconversion Properties. A typical energy level diagram for the upconverted emission from a sample codoped with Yb^{3+} and Er^{3+} ions under infrared excitation is shown in Figure 3. The upconverted fluorescence spectra of the Er^{3+}:ZrO_2 nanocrystals in different concentrations of Er^{3+} are shown in Figure 4. A significant drop in the overall intensity and a change in the spectral nature of these bands is observed with an increasing concentration of Er^{3+} ions. The relative increase in intensity of red emission with respect to the intensity of green emission was observed with an increasing concentration of erbium. The mechanism of the upconverted emission of Er^{3+} has been well established in the literature.[3−6] The diode-laser wavelength matches the absorption transition between the ground state, $^4I_{15/2}$, and the excited level $^4I_{11/2}$. After first-level excitation, the same laser pumps the excited atom from the $^4I_{11/2}$ to the $^4F_{7/2}$ level. Subsequent nonradiative relaxation populates the $^4S_{3/2}$/ $^2H_{11/2}$ and the $^4F_{9/2}$ levels. Bright green (550 nm) and red (675 nm) emission were observed due to the transitions

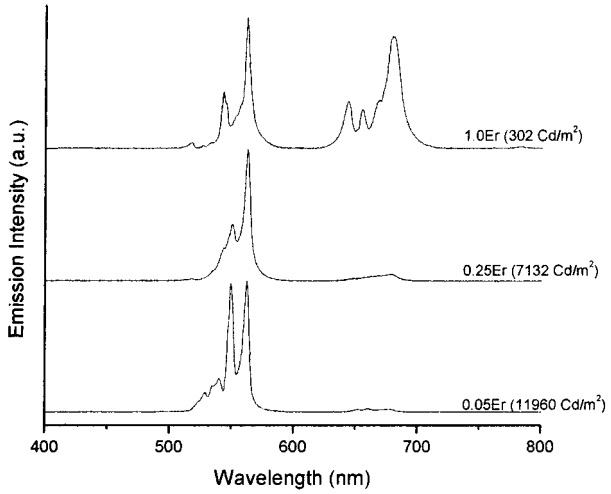

Figure 4. Upconverted emission spectra of different concentrations of Er^{3+} in ZrO_2 nanoparticles heated at 1000 °C.

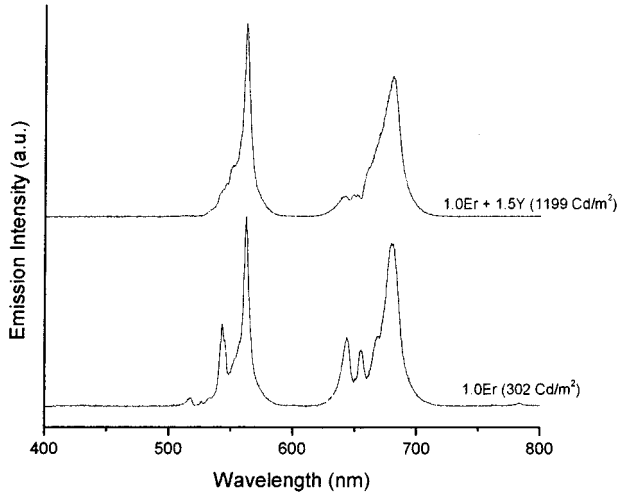

Figure 5. Upconverted emission spectrum of Er^{3+} doped in Y^{3+}:ZrO_2 nanoparticles heated at 1000 °C.

$^4S_{3/2} \rightarrow {}^4I_{15/2}$ and $^4F_{9/2} \rightarrow {}^4I_{15/2}$, respectively.[3−8] At low concentration, the erbium ions are usually randomly distributed in the host lattice but at higher concentration, some of the Er^{3+} ions have a closer nearest neighbor than others and concentration quenching can occur. At low dopant concentration, the $^4S_{3/2}$/ $^2H_{11/2}$ levels decay mostly radiatively to $^4I_{15/2}$. Therefore, the green emission has a higher intensity. It is reported[5] that at a higher concentration, the luminescent lifetime of $^4S_{3/2}$/ $^2H_{11/2}$ levels is shortened as a result of the cross-relaxation (CR) processes between ($^2H_{11/2} \rightarrow {}^4I_{9/2}$) and ($^4I_{15/2} \rightarrow {}^4I_{13/2}$) transitions as shown in Figure 3. This cross-relaxation process is dominant at higher concentrations of Er^{3+} ions. Therefore, quenching of emission takes place at higher concentrations of erbium ions.

Figure 5 shows the upconverted spectra of Y^{3+}-codoped Er^{3+} in ZrO_2 samples. A significant increase of the upconverted emission in the presence of Y^{3+} may be due to better miscibility of Er^{3+} in yttrium-codoped zirconia, which hinders the creation of large clusters[16] and circumvents the concentration quenching process for the same concentration of Er^{3+}. There is a possibility for the existence of erbium ions in either the yttrium or zirconium lattice site that prevents the aggregation resulting in the circumvention of the nonradiative process ($^2H_{11/2} \rightarrow {}^4I_{9/2}$)/ ($^4I_{15/2} \rightarrow {}^4I_{13/2}$) due to cross relaxation. Therefore, $^4S_{3/2}$/ $^2H_{11/2}$ levels decay mostly radiatively to the $^4I_{15/2}$ level and an overall increase in intensity is observed.

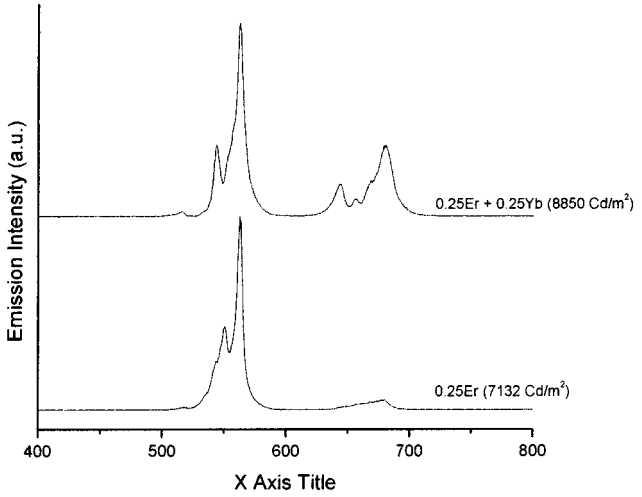

Figure 6. Upconverted emission spectrum of Er^{3+} doped in Yb^{3+}:ZrO_2 nanoparticles heated at 1000 °C.

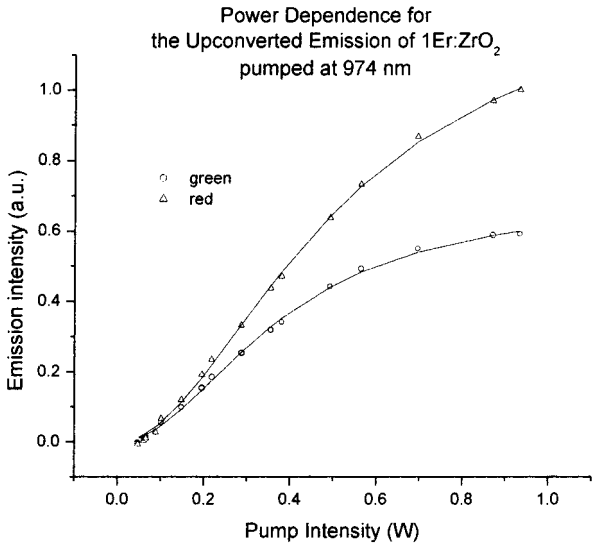

Figure 7. Variation of red and green upconverted emission intensities with pump power for 1.0 Er^{3+}:ZrO_2 sample.

Figure 6 presents the upconverted spectra of Er^{3+}:ZrO_2 codoped with Yb^{3+}. In this system there can be three mechanisms for upconversion. The first possibility is simple excited-state absorption (ESA), where Yb^{3+} ions do not play any role. A second possibility is energy transfer upconversion (ETU), where two excited ($^4I_{11/2}$) Er^{3+} ions interact with each other and one ion is de-excited to $^4I_{15/2}$ and the other is excited to $^4F_{7/2}$. This mechanism can be described as

$$2^4I_{11/2} \rightarrow {}^4I_{15/2} + {}^4F_{7/2}$$

A third mechanism for upconversion is energy transfer from Yb^{3+} ($^2F_{5/2}$) to Er^{3+} ($^4I_{11/2}$).[6] The ET from Yb^{3+} ($^2F_{5/2}$) to Er^{3+} ($^4I_{11/2}$) depends on the Yb^{3+} concentration, i.e., the transfer process depends on the donor and acceptor concentration.[6] During the lifetime of the $^4I_{11/2}$ level a second photon is absorbed by Yb^{3+} and energy transferred to Er^{3+}. The Er^{3+} is now raised from $^4I_{11/2}$ to $^4F_{7/2}$. The possible channels for the green and red upconversion luminescence are given below:

$$^2F_{5/2}\,(Yb^{3+}) + {}^4I_{11/2}\,(Er^{3+}) \rightarrow {}^2F_{7/2}\,(Yb^{3+}) + {}^4F_{7/2}\,(Er^{3+})$$

The $^4F_{7/2}$ (Er^{3+}) state decays nonradiatively to the $^4S_{3/2}$/ $^2H_{11/2}$ and $^4F_{9/2}$ (Er^{3+}) levels. The green emission is observed from

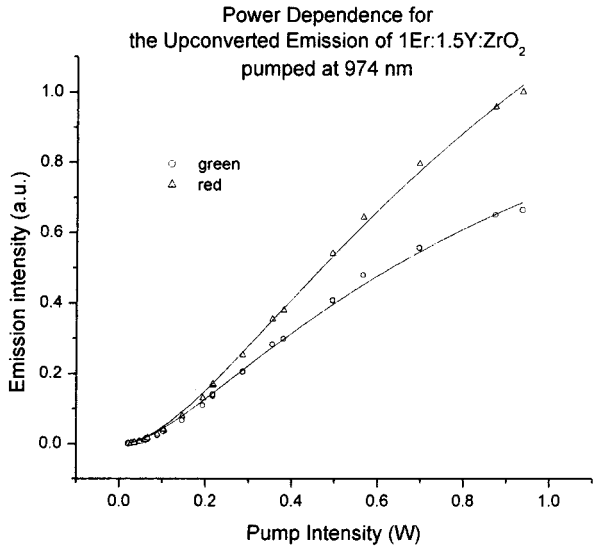

Figure 8. Variation of red and green upconverted emission intensities with pump power for 1.0 Er^{3+}:1.5 Y^{3+}:ZrO_2 sample.

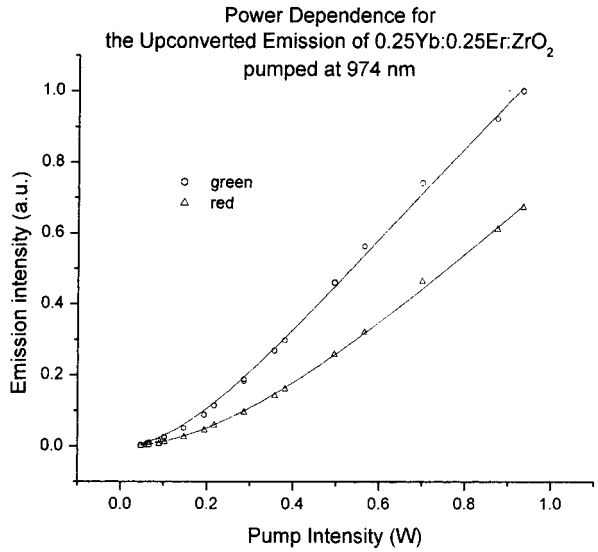

Figure 9. Variation of red and green upconverted emission intensities with pump power for 0.25 Er^{3+}:0.25 Yb^{3+}:ZrO_2 sample.

the $^4S_{3/2} \rightarrow {}^4I_{15/2}$ transition while the $^4F_{9/2} \rightarrow {}^4I_{15/2}$ transition produces red emission. This is also confirmed by the observed increase in overall emission intensity in the presence of Yb^{3+} with Er^{3+}.

The variations of the fluorescence intensity of the green and red emission versus pump intensity in various compositions are plotted in Figures 7−9. For a two-photon ETU/ESA upconversion process, the fluorescence intensity should be related to the pump intensity by the following equation:[17]

$$I_f = \frac{KI_p^2}{(A + BI_p + CI_p^2)} \qquad (2)$$

where all the coefficients are always positive. I_f is the upconverted fluorescence intensity and I_P is the pumping intensity. K is a constant that depends on collection geometry and the Er^{3+} density in the sample. A, B, and C are constants related to the transition probabilities, and the absorption cross-section of the involved transitions. It can be seen in Figure 7−9 that eq 2 fits excellently to all sets of experimental data. These results confirm that the upconversion in all these materials is due to two-photon ESA/ETU processes.

4. Conclusions

We have shown that the overall upconversion luminescence intensity decreases with an increasing concentration of the Er^{3+} ions in a ZrO_2 matrix. We suggest that concentration quenching is responsible for the decrease in overall intensity. In the presence of Y^{3+} ions the overall upconversion emission intensity of Er^{3+} was found to increase. The Y^{3+} ions are presumed to prevent the cluster formation of erbium ions and therefore, the nonradiative path due to concentration quenching is reduced resulting in an increase in the upconverted emission intensity of Er^{3+}. The Yb^{3+} ions, which act as a sensitizer, also enhance the upconversion luminescence under infrared excitation. We have also confirmed that the upconversion process in all these materials results from two-photon ESA/ETU processes.

Acknowledgment. This work was supported in part by the Air Force Office of Scientific Research, The Directorate of Chemistry and Life Sciences through a DURINT grant (#F496200110358) and in part by NSF, DMR solid state chemistry grant (#DMR 0075867).

References and Notes

(1) Silversmith, A. J.; Lenth, W.; Macfarlane, R. M. *Appl. Phys. Lett.* **1987**, *51*, 1977.
(2) Maciel, G. S.; de Araujo, C. B.; Messaddeq, Y.; Aegerter, M. A. *Phys. Rev. B* **1997**, *55*, 6335.
(3) Kapoor, R.; Friend, C. S.: Biswas, A.; Prasad, P. N. *Opt. Lett.* **2000,** *25*, 338.
(4) Pollnau, M.; Gamelin, D. R.; Luthi, S. R.; Gudel, H. U.; Hehlen, M. P. *Phys. Rev. B* **2001**, *61*, 3337.
(5) Golding, P. S.; Jackson, S. D.; King, T. A.; Pollnau, M. *Phys. Rev. B* **2000**, *62*, 856.
(6) Silver, J.; Martinez-Rubio, M. I.; Ireland, T. G.; Fern, G. R.; Withnall, R. *J. Phys. Chem. B* **2001**, *105*, 948.
(7) Yi, G. C.; Block, B. A.; Ford, G. M.; Wessels, B. W. *Appl. Phys. Lett.* **1998**, *73*, 1625.
(8) Zhang, H. X.; Kam, C. H.; Zhou, Y.; Han, X. Q.; Buddhudu, S.; Xiang, Q.; Lam, Y. L.; Chan, Y. C. *Appl. Phys. Lett.* **2000**, *77*, 609.
(9) Reisfeld, R.; Jorgensen, C. K. *Laser and Excited state of rare-earths*; edited Reisfeld, R., Jorgensen, C. K., Eds.; Springer-Verlag: Berlin, 1977.
(10) Reisfeld, R.; Zelner, M.; Patra, A. *J. Alloys Compd.* **2000**, *300−301*, 147.
(11) Schmidt, T.; Muller, G.; Spanhel, L.; Kerkel, K.; Forchel, A. *Chem. Mater.* **1998**, *10*, 65−71.
(12) Chatterjee, M.; Naskar, M. K.; Siladitya, B.; Ganguli, D. *J. Mater. Res.* **2000**, *15*, 176.
(13) Chatterjee, M.; Patra, A. *J. Am. Ceram. Soc.* **2001**, *84* (7), 1439.
(14) Masui, T.; Fujiwara, K.; Machida, K.; Adachi, G.; Sakata, T.; Mori, H. *Chem. Mater.* **1997**, *9*, 2197.
(15) Lisiecki, I.; Bjorling, M.; Motte, L.; Ninham, B.; Pileni, M. P. *Langmuir* **1995**, *11*, 2385.
(16) Gedanken, A.; Reisfeld, R.; Sominski, E.; Palchik, O.; Koltypin, Yu.; Panczer, G.; Gaft, M.; Minti, H. *J. Phys. Chem. B* **2000**, *104*, 7057.
(17) Kapoor, R.; Friend, C.; Patra, A.; Prasad, P. N. To be submitted.